Eleventh U.S. National Conference on Earthquake Engineering
Integrating Science, Engineering & Policy
June 25-29, 2018
Los Angeles, California

FIBER-BASED MODEL FOR EARTHQUAKE-IDNUCED COLLAPSE SIMULATION OF STEEL FRAME BUILDINGS

Y. Suzuki[1] and D. Lignos[2]

ABSTRACT

Earthquake-induced collapse risk assessment of steel frame buildings requires the use of simulation models that can realistically replicate dynamic instability of frame buildings. Such models for steel columns should consider the coupling between the axial force and flexural demands. In end columns, the axial load demand variations due to dynamic overturning effects may be considerable. Other important aspects to be considered are the cyclic hardening prior to the onset of local buckling; the column post-buckling behavior under various axial and lateral loading histories. The potential of utilizing different steel materials should also be considered.

This paper proposes a component model that simulates the hysteretic behavior of steel columns utilizing hollow structural sections at large deformations. A fiber-based approach is adopted that combines an equivalent engineering stress-strain constitutive relation assigned to a fiber cross-section within a pre-defined plastic hinge length of a force-based beam-column element formulation. The pre- and post-buckling behavior of the equivalent engineering stress-strain relation is defined based on uniaxial cyclic coupon tests and extensive stub column finite element analyses. The effectiveness of the proposed model in simulating the steel column behavior is demonstrated through comparisons with steel column collapse experiments as well as frame simulation studies validated with shake table collapse tests.

[1]Senior Researcher, Nippon Steel and Sumitomo Metal Corporation, Janan, suzuki.s2k.yusuke@jp.nssmc.com
[2]Associate Professor, Swiss Federal Institute of Technology, Lausanne (EPFL), Switzerland, dimitrios.lignos@epfl.ch

Lord J, Wright R. Template to illustrate paper format for the 11NCEE. *Proceedings of the 11th National Conference in Earthquake Engineering*, Earthquake Engineering Research Institute, Los Angeles, CA. 2018.

Fiber-Based Model for Earthquake-Induced Collapse Simulation of Steel Frame Buildings

Y. Suzuki[1] and D. Lignos[2]

ABSTRACT

Earthquake-induced collapse risk assessment of steel frame buildings requires the use of simulation models that can realistically replicate dynamic instability of frame buildings. Such models for steel columns should consider the coupling between the axial force and flexural demands. In end columns, the axial load demand variations due to dynamic overturning effects may be considerable. Other important aspects to be considered are the cyclic hardening prior to the onset of local buckling; the column post-buckling behavior under various axial and lateral loading histories. The potential of utilizing different steel materials should also be considered.

This paper proposes a component model that simulates the hysteretic behavior of steel columns utilizing hollow structural sections at large deformations. A fiber-based approach is adopted that combines an equivalent engineering stress-strain constitutive relation assigned to a fiber cross-section within a pre-defined plastic hinge length of a force-based beam-column element formulation. The pre- and post-buckling behavior of the equivalent engineering stress-strain relation is defined based on uniaxial cyclic coupon tests and extensive stub column finite element analyses. The effectiveness of the proposed model in simulating the steel column behavior is demonstrated through comparisons with steel column collapse experiments as well as frame simulation studies validated with shake table collapse tests.

Introduction

Due to capacity design considerations, steel columns in moment resisting frames (MRFs) are expected to remain elastic during an earthquake. Variations in material properties and the moment gradient due to force redistributions within a MRF may cause flexural yielding and/or inelastic buckling in steel columns. Therefore, their inelastic behavior should be appropriately represented within a building numerical model. In particular, the column axial force and bending interaction (i.e., P-M interaction) is critical especially in end columns that may experience axial load demand variations due to overturning effects. The cyclic hardening prior to the onset of local buckling depending on the steel material is also important. For earthquake-induced collapse simulations the column post-buckling behavior should be properly represented. A number of phenomenological models were developed and employed for modeling ultimate limit states in steel structural components (e.g., [1, 2]). These models successfully reproduced collapse of steel MRFs [3]. Prior studies associated with the hysteretic behavior of steel columns indicate that a number of limit states are not properly addressed by the aforementioned models [4, 5]. These

[1] Senior Researcher, Nippon Steel and Sumitomo Metal Corporation, Japan, suzuki.s2k.yusuke@jp.nssmc.com
[2] Associate Professor, Swiss Federal Institute of Technology, Lausanne (EPFL), Switzerland, dimitrios.lignos@epfl.ch

Lord J, Wright R. Template to illustrate paper format for the 11NCEE. *Proceedings of the 11th National Conference in Earthquake Engineering*, Earthquake Engineering Research Institute, Los Angeles, CA. 2018.

include column axial shortening and its progression. With the advent of material science, high-performance steel materials have been developed for seismic applications [6] that potentially reduce the earthquake-induced collapse risk of steel frame buildings. Therefore, steel column deterioration models should be versatile and capture this aspect.

This paper proposes a component model that simulates the hysteretic behavior of steel hollow structural section (HSS) columns at large deformations. A fiber-based approach is adopted that combines an equivalent engineering stress-strain constitutive relation that is defined over a plastic hinge length. This relation is assigned to a fiber cross-section of HSS within a plastic hinge length of a force-based beam-column element formulation. The pre- and post-buckling behavior of the equivalent engineering stress-strain relation is defined based on uniaxial cyclic coupon tests and virtual stub column experiments conducted with finite element (FE) analysis. The proposed model is validated with available steel column collapse experiments and frame simulation studies validated with shake table collapse tests.

Concept of fiber modeling approach

Fig. 1 illustrates the concept of the proposed modeling approach. In order to capture the pre- and post-buckling behavior of the steel HSS columns, a plastic hinge length equivalent to the buckling length of the column is defined at the column end. A fiber section is assigned to the presumed finite length. The buckling length is set to 0.8D (D is the HSS column depth) based on prior work [4, 5, 7]. The fiber section can contract/elongate depending on the combined axial and flexural force that shifts the neutral axis of the respective cross section (see Fig. 1b). One of the main challenges is to develop a realistic engineering stress-strain relation that is assigned to a discretized fiber cross section. The stress-strain relation should capture: strain hardening in the pre-buckling limit state; strength deterioration in the post-buckling limit state under monotonic loading and cyclic/in-cycle deterioration in flexural strength under cyclic loading histories. These issues are elaborated in the subsequent sections.

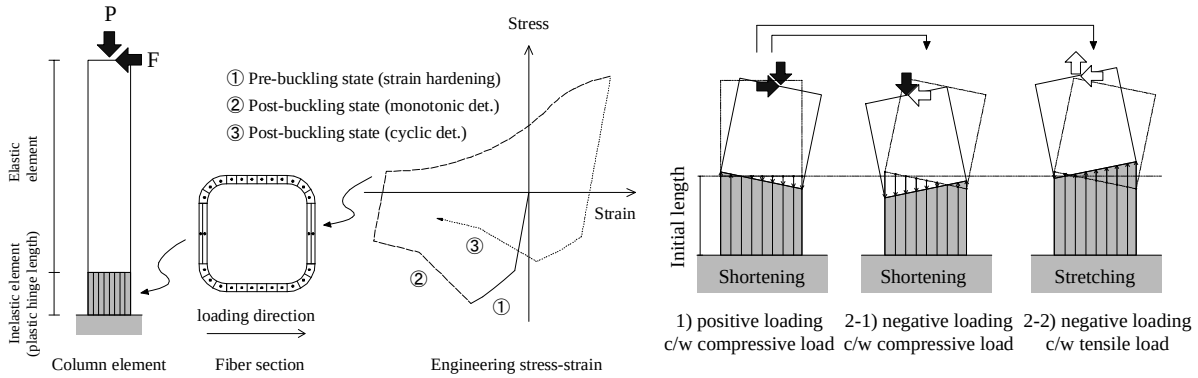

(a) modeling overview (b) schematic of axial shorteinng

Figure 1. Concept of fiber modeling approach

Pre-peak behavior

The emphasis of this research is to develop models for HSS columns. Therefore, rectangular and circular coupons are extracted from different locations of an HSS column. These coupons are

subjected to uniaxial monotonic and cyclic load such that the material isotropic/kinematic strain hardening can be fully characterized. Full-thickness rectangular specimens are extracted from the HSS's flat and corner section and they are subjected to monotonic tensile load. Round bar specimens are taken from the flat cross-section and they are subjected to uniaxial cyclic load. Referring to Fig. 2, the true stress-strain curves of ASTM A500 steel are shown. The stress-strain evolution in the pre-peak response is represented with a nonlinear kinematic and isotropic hardening model proposed by [8], which is also available in commercial continuum finite element codes. One backstress is assumed in this case. In brief, the kinematic hardening component is calibrated to fit the monotonic tensile coupon test. The isotropic hardening component is then calibrated to fit the cyclic stress strain relation. The corner cross-section does not exhibit isotropic hardening due to pre-straining during the manufacturing process. The predicted stress-strain curves based on the identified hardening parameters are superimposed in Fig. 2. From these figures, it is seen that the predicted stress-strain relations capture the inelastic behavior of the steel material.

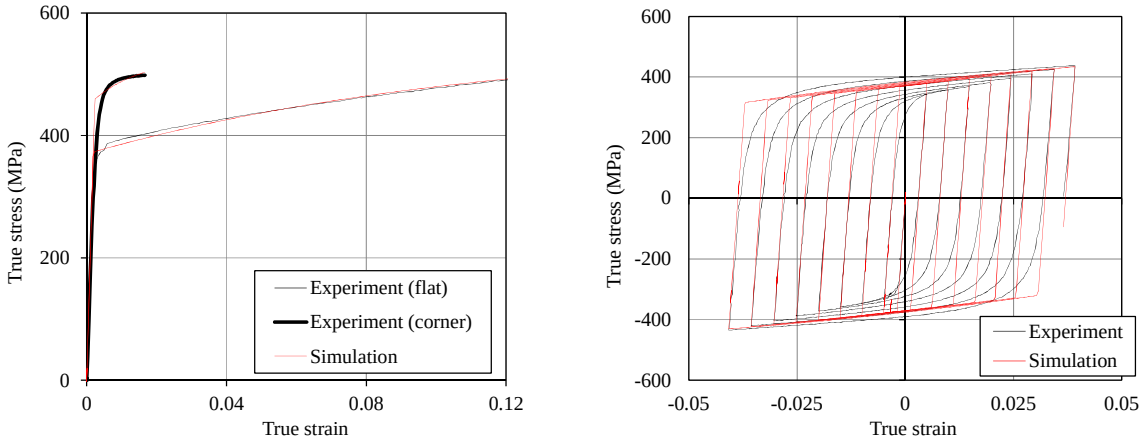

(a) monotonic load (b) cyclic load

Figure 2. Stress strain curves of ASTM A500 steel

Post-peak behavior

In order to simulate post-buckling behavior of HSS columns, the stress-strain formulation shall contain a softening branch such that the effects of local buckling can be inherently captured within the fiber formulation. For this purpose, the stress-strain formulation can be defined by uniaxial stub column tests. Virtual FE experiments are conducted for this purpose. The main parameter that is varied is the HSS column depth-to-thickness ratio (D/t). Fig. 3 illustrates an overview of the FE model employed for the stub column virtual experiments. The FE model is developed in the FE package ABAQUS [9]. The HSS stub column height is three times the column depth. The HSS member is modeled with a shell element (S4R). Uniaxial load is applied on the rigid element at the HSS section top. The true stress-strain relations shown in the previous section are assigned to the FE model. Referring to Fig. 3a, residual stress distributions are considered based on the model proposed by [10]. In order to trigger local geometric instabilities in the FE analysis, (i.e., local buckling), a geometric imperfection proportional to the first eigen mode is introduced. The imperfection is scaled such that the maximum out-of-plane displacement Δ of the local buckling is 0.2% of the HSS depth excluding the corner section. The

yield stress of the HSS flat section is based on the nominal yield stress. The yield stress of the corner section is defined based on the assumption that it is typically 100MPa higher than that of the flat section (see Fig. 2a). The equivalent strain is extracted from the buckled region by assuming a plastic hinge length equal to 0.8*D*. Fig. 3b shows the equivalent engineering stress-strain relation of the HSS stub column subjected to monotonic compressive axial load. The equivalent stress caps due to local buckling in all cases. If the section becomes more compact, the capping stress and yield-to-capping strain increase. The post-peak deterioration slope is initially steep but gradually becomes flat due to stabilization of the local buckling wave [7, 11].

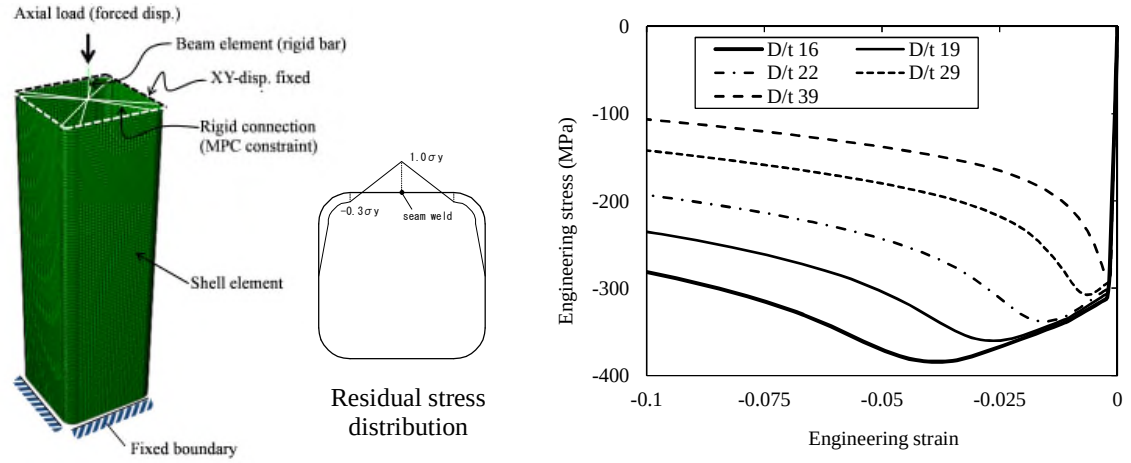

(a) Overview of the FE model (b) Equivalent stress-strain curves

Figure 3. Overview of the FE stub column model and equivalent stress-strain curves under monotonic compressive loading

Fig. 4 shows the equivalent stress-strain relations obtained from HSS stub column FE simulations subjected to uniaxial cyclic loading. Note that the compressive stress deteriorates cyclically due to local buckling within the stub column length. When the constant strain amplitude is employed, the post-capping deterioration slope as well as the residual stress of the HSS members is stabilized. This is to be expected based on prior experimental studies [11]. The stress in tension keeps increasing while reloading and it exceeds the previous peak stress during the incremental strain amplitude. This is why the out-of-plane distortion of the HSS member due to local buckling is stretched during the reloading stage. During the constant amplitude protocol, accelerated reloading stiffness deterioration becomes more significant. As such, the reloading stress does not exceed the previous peak value. This is because the buckling wave of the HSS members does not fully stretch during the reloading stage at constant strain amplitude. The next loading process in compression increases the buckling wave. The unloading stiffness in compression deteriorates during both incremental and constant strain amplitude protocols. The unloading stiffness in tension during the incremental strain amplitude does not deteriorate as much as in compression. But the unloading stiffness in tension during constant strain amplitude does. The reason is that the buckling wave is fully stretched under tensile load during the incremental strain amplitude because the stress exceeds the previous stress peak. If the buckling wave is not fully stretched during the tensile excursion (i.e., during constant strain amplitude), the remained out-of-plane displacement is the reason that the column stiffness deteriorates.

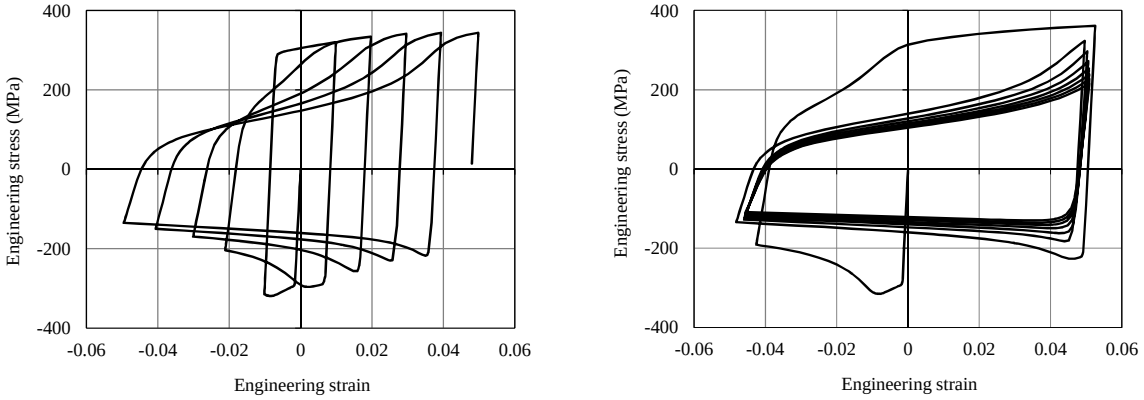

(a) incrementally cyclic loading (b) constant amplitude cyclic loading

Figure 4. Stress strain curves of HSS stub column subjected to cyclic load (D/t=29)

Development of equivalent engineering stress-strain relation

To fully define the observed stress strain relation discussed earlier, a monotonic backbone curve of the equivalent engineering stress-strain relation is developed at first. Then the effects of cyclic deterioration on the monotonic curve are considered.

Modeling of monotonic backbone curve

Fig. 5a illustrates a schematic representation of the monotonic stress-strain relation. The monotonic stress-strain curve in compression consists of three main parts; the elastic, the post-yield and the post-capping region. In the elastic region, the elastic modulus, E_m, is normally 200GPa for commonly used steel materials. In the post-yield region, the yield stress, $\sigma_{y,m}$, is defined based on the yield stress of the flat section of HSS. The strain hardening is determined in the same way as we discussed in the previous section, i.e., a combined strain hardening is determined. This hardening evolution law is defined from a true stress strain relation (see Fig. 2). In the post-capping region, the capping stress and pre-capping strain, $\sigma_{c,m}$ and $\varepsilon_{c,m}$, respectively, are first defined. After capping, two post-capping slopes, $E_{d1,m}$ and $E_{d2,m}$, are defined. The stress at the intersection of the first and second slope is defined as, $\sigma_{d,m}$. The second post-capping slope, $E_{d2,m}$ is smoother than the first one right after stress capping (i.e., $E_{d1,m}$). This represents the post-capping slope after stabilization of the local buckling wave at large strains [11]. All the parameters after stress capping in compression can be fully defined based on steel stub column compressive tests. In the tensile loading direction, only the elastic and post-yield behavior should be defined based on a standard tensile coupon test. In order to predict how the post-capping parameters change per column section slenderness, regression equations are developed. A general functional form shown below is used for this purpose,

$$CP = a\left(\frac{D}{t}\right)_{eq}^{b}, \left(\frac{D}{t}\right)_{eq} = \left(\frac{D}{t}\right)\sqrt{\varepsilon_{y,m}} \quad (1)$$

in which, CP is the configuration parameter to be predicted (i.e., $\sigma_{c,m}$, $\varepsilon_{c,m}$, $E_{d1,m}$, $E_{d2,m}$, $\sigma_{d,m}$); coefficients a and b are determined based on standard regression analysis from stub column

compressive tests; D/t is the column depth-to-thickness ratio; and $\varepsilon_{y,m}$ is the yield strain.

Modeling of cyclic deterioration

Figs. 5b and 5c illustrate a schematic representation of the hysteresis modeling approach for cyclic deterioration. In compression, the unloading stiffness $E_{u,c}$, yield stress $\sigma_{y,c}$, capping stress $\sigma_{c,c}$, pre-capping strain $\varepsilon_{py,c}$, the post-capping deterioration slopes $E_{d1,c}$ and $E_{d2,c}$ are defined. These parameters are updated based on the extent of inelastic damage with reference to the monotonic stress-strain relation. In particular, the post-capping slopes are defined based on a straight-line approximation. The post-yield slope is approximated by a smooth curve based on the Ramberg-Osgood function [12]. This curve is determined from the unloading stiffness, $E_{u,c}$ of the stress strain curve and a coefficient n_c that determines the smoothness of the curve. In the tensile excursion, the unloading stiffness $E_{u,t}$ and yield stress $\sigma_{y,t}$ are determined in a similar manner. The stress and strain for the pinching point, $\sigma_{p,t}$ and $\varepsilon_{p,t}$ are then defined. The reloading slope connecting the yield-to-pinching point is defined based on a Ramberg-Osgood function. This is based on the stiffness at the pinching point, $E_{p,t}$ and coefficient n_t. After this point, there is a smooth transition of the stress strain curve to the strain-hardening region. After the pinching point, both the stress and the strain are determined by the combined hardening law that is employed in the pre-capping region.

It was found that the total strain and the strain amplitude control the cyclic behavior of a stub column. This agrees with earlier findings by [11]. Cyclic deterioration is also influenced by the section local slenderness, D/t. Referring to Fig. 5, the peak strain ratio and the peak stress ratio are defined. In this figure, it is assumed that the previous peak is the point at which the buckling wave is fully stretched. The peak strain ratio explains how far the unloading starts in tension from the previous peak. If the peak strain ratio becomes larger, local buckling is extensive that results to more deterioration. The peak stress ratio explains how much more of the buckling wave remains when the unloading starts in compression. If the peak stress ratio becomes smaller, then the buckling wave remains in the HSS member and the stress-strain relation deteriorates more. If unloading starts after exceeding the previous peak stress, it is assumed that the buckling wave is fully stretched. In this case, the peak stress ratio is assumed to be 1.0.

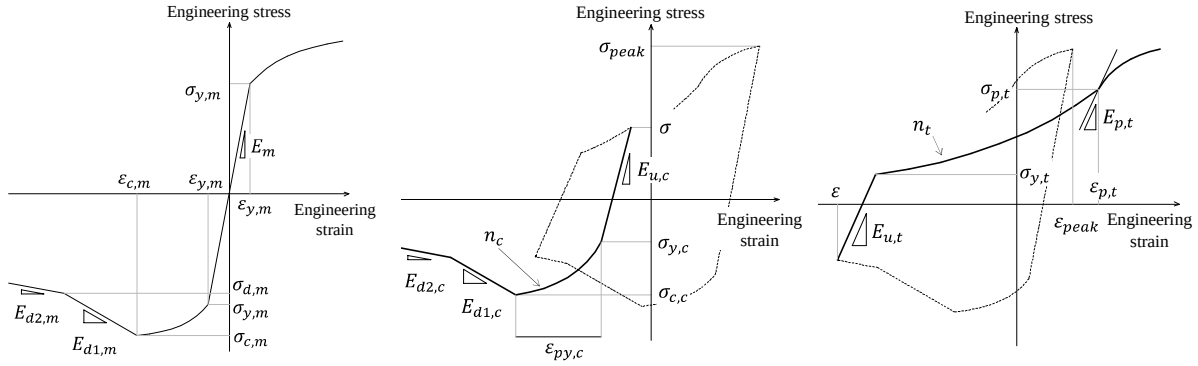

(a) back bone curve (b) compressive excursion (c) tensile excursion

Figure 5. Schematic of equivalent stress-strain relation for monotonic and cyclic loading

Verification with component tests

The proposed equivalent stress-strain material model is assigned to a fiber discretization. The fiber cross-section is utilized within a plastic length of a force-based element formulation [13]. A force-based formulation is preferred over a displacement-based one because in the former the internal element interpolation functions represent accurately the force equilibrium with just one element [14]. The mid-point integration scheme [15] is employed because the maximum flexural demands within the column typically occur away from the column base [4, 5] and near the center of the assumed plastic hinge length. Using the modeling methodology discussed above, a verification study of the proposed element is conducted. Fig. 6 shows a comparison of the measured and simulated moment and axial shortening versus chord rotation of HSS254x9.5 subjected to collapse-consistent loading protocols [4, 16]. Both constant and varying axial loads are coupled with the lateral loading history such that the loading conditions of typical interior and end steel MRF columns are properly represented, respectively. Referring to Fig. 6, the proposed model is able to simulate reasonably well the cyclic deterioration in flexural strength of the steel column regardless of the employed loading history as well as the cyclic hardening prior to the formation of local buckling. The proposed deterioration model is also able to simulate relatively well the column axial shortening under both constant and varying axial loading conditions. Further verification studies are currently conducted based on detailed FE studies of beam-columns subjected to various loading histories.

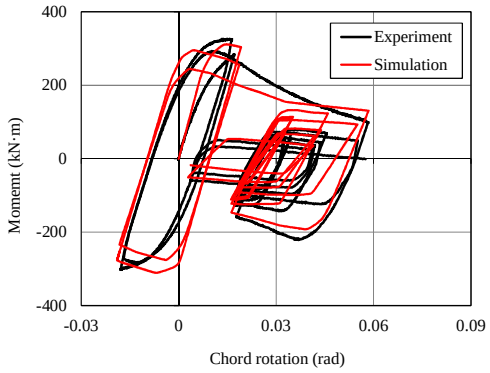

(a) moment-rotation, const. axial load

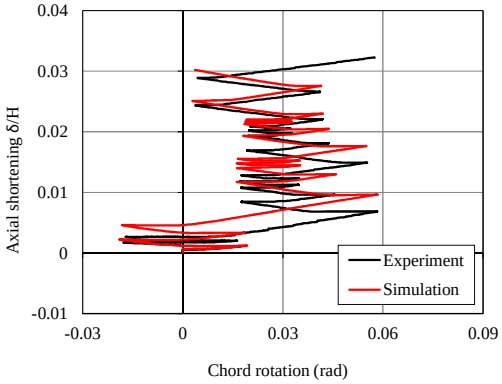

(b) axial shortening-rotation, const. axial load

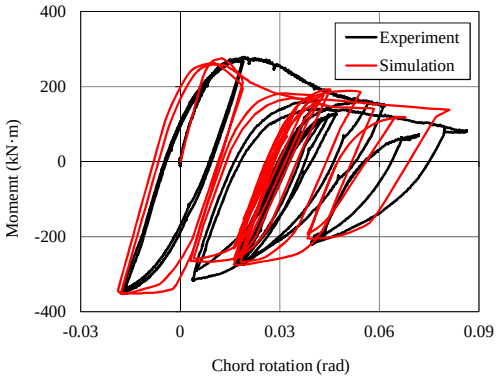

(c) moment-rotation, var. axial load

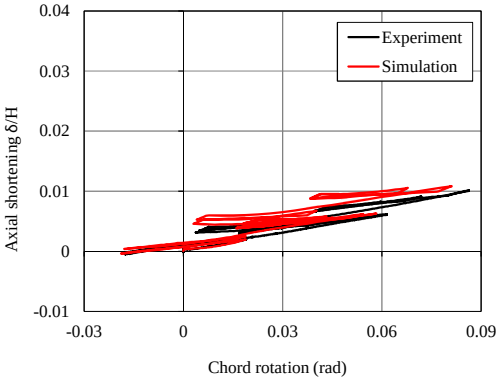

(d) axial shortening-rotation, var. axial load

Figure 6. Verification result of HSS254x9.5 subjected to collapse-consistent loading protocols

Simulation of E-defense 4-story steel MRF collapse test

In this section, a frame analysis verification is conducted to demonstrate the efficiency of the proposed model for collapse simulations. The results of the 4-story steel building tested at full-scale through collapse at E-Defense is employed for this purpose [17]. A 2-dimentional 2-bay frame (Y-direction frame) model is developed in the Open System for Earthquake Engineering Simulation (OpenSees) platform [18]. Steel columns are modeled with the proposed element discussed herein. Steel beams are modeled with the modified Ibarra-Medina-Krawinkler (IMK) model [1]. The panel zone shear distortion is modeled with the Krawinkler trilinear model [19]. The composite action effects are considered as discussed in [20]. Viscous damping is approximated with the Rayleigh damping model. The assumed damping ratio is 2% at the first period, T_1 and at $0.25T_1$ of the corresponding steel MRF. The scaled intensities (40, 60, and 100%) of JR Takatori ground motion are applied sequentially to the numerical model. Fig. 7 shows a comparison of the simulated and the measured response at the unscaled JR Takatori seismic intensity. Both the story drift ratio (SDR) and the column moment-rotation relation prior to collapse are predicted relatively well.

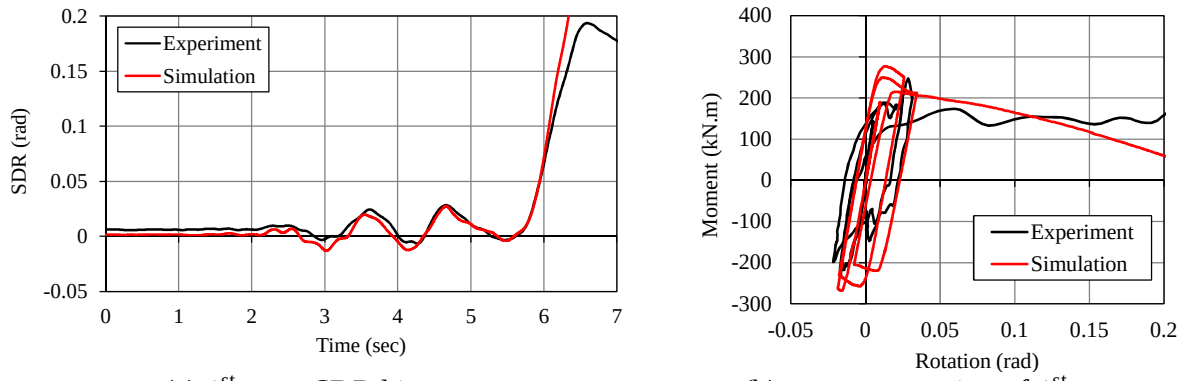

(a) 1st story SDR history

(b) moment-rotation of 1st story interior column base

Figure 7. Responses of E-defense shake table test during 100% scaled intensity

Fig. 8 illustrates the responses of the first-story columns during the same seismic intensity. The end columns are noted as column 1 and 3. Column 2 is the interior one. From Fig. 8a, strength deterioration of the interior column is observed during the positive and negative loading directions. On the other hand, end columns deteriorate only in the compressive loading direction. Referring to Fig. 8b, the interior column axial shortening accumulates during cyclic loading. On the other hand, the end column axial shortening varies linearly with respect to the column rotation. Therefore, a differential gap of 10mm between columns 1 and 2 develops prior to collapse. Referring to Fig. 8c, the axial load on the interior column is slightly reduced during the inelastic cycles. This is due to the load redistribution attributed to the axial shortening that grows more in interior columns. The observed differences of the interior and end column behavior are consistent with prior experimental studies conducted by the authors [4, 5]. The observed differential gap due to axial shortening is expected to tilt the floor system. The collapse simulation herein demonstrates the importance of capturing the P-M interaction and the column axial shortening in addition to strength and stiffness deterioration when local engineering demand parameters are of interest.

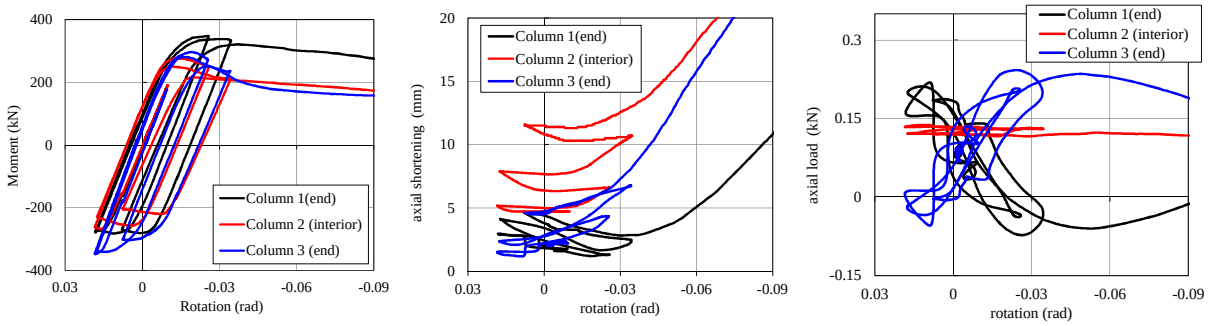

(a) moment-rotation (column base) (b) axial shortening-rotation (c) axial load-rotation

Figure 8. Responses of 1st story columns during 100% scaled intensity

Summary

This paper summarized the development of a deterioration model for steel HSS columns subjected to multi-axis cyclic loading. The proposed model is able to capture the axial load-flexural strength interaction and growth of axial shortening as well as strength and stiffness deterioration due to local buckling. An equivalent engineering stress-stain constitutive relation is developed based on standard mechanical tests. This curve inherently captures local buckling based on a softening branch. The stress-strain formulation is assigned to a fiber cross-section that in turn is assigned to a plastic hinge length within a force-based element formulation. The proposed model is validated with steel HSS beam-column tests subjected to collapse-consistent loading protocols. The efficiency of the proposed model is also demonstrated in predicting the dynamic response of a 4-story steel MRF that was tested through collapse. The major findings of the paper are summarized as follows:

- The kinematic/isotropic hardening characteristics of a steel material prior to local buckling within a steel cross section are identified based on standard uniaxial coupon tests directly extracted from the flat and corner parts of the HSS. This provides versatility to utilize any steel material of interest.
- The post-peak response of the equivalent stress-strain formulation is quantified on the basis of stub column tests. This formulation is characterized by stress capping in compression; reloading in tension; cyclic deterioration in strength and stiffness; local buckling stabilization.
- The developed equivalent engineering stress-strain formulation is extracted over the length that local buckling forms. Typically, this length is $0.8D$ for HSS columns. For a more appropriate formulation, the yield-to-capping path in compression and the yield-to-pinching path in tension are described with a Ramberg-Osgood function to trace the smooth transition of the stress strain curve to the strain-hardening region.
- The proposed equivalent stress-strain formulation is assigned to a fiber cross section that is in turn assigned over a plastic hinge length of a nonlinear beam-column element. The proposed model is able to simulate reasonably well the moment-rotation and axial-shortening that accumulates with the local buckling progression.
- Collapse simulations suggest that the proposed model is able to capture the local damage and its progression within an actual steel MRF system. It was found that interior columns

may shorten more than end columns within the same steel MRF story. This may cause slab tilting prior to collapse. This issue deserves more attention in future studies associated with earthquake-induced collapse. The authors are currently working into this direction.

References

1. Ibarra LF, Medina RA, Krawinkler H. Hysteretic models that incorporate strength and stiffness deterioration. *Earthquake Engineering & Structural Dynamics*, 2005; 34(12): 1489–1511.
2. Sivaselvan M, Reinhorn A. Hysteretic models for deteriorating inelastic structures. *Journal of Engineering Mechanics*, 2005; 126(6): 633–640.
3. Lignos DG, Hikino T, Matsuoka Y, Nakashima M. Collapse assessment of steel moment frames based on E-Defense full-scale shake table collapse tests. *Journal of Structural Engineering*, 2013; 139 (1): 120-132.
4. Suzuki Y, Lignos DG. Collapse behavior of steel columns as part of steel frame buildings: experiments and numerical models. *16th World Conference on Earthquake (WCEE)*, Santiago Chile, 2017.
5. Suzuki Y, Lignos DG. Large scale collapse experiments of wide flange steel beam-columns. *8th International Conference on Behavior of Steel Structures in Seismic Areas (STESSA)*, Shanghai, China, 2015.
6. Kanno R. Advances in steel materials for innovative and elegant steel structures in Japan – A review. *Structural Engineering International*, IABSE, 2016; 26(3): 242-253.
7. Yamada S, Akiyama H, Kuwamura H. Post-buckling and deteriorating behavior of box-section steel members. *Journal of Structural and Construction Engineering*, AIJ, 1993; 444: 135–143. (in Japanese)
8. Lemaitre J, Chaboche JL. A non-linear model of creep-fatigue damage cumulation and interaction (for hot metallic structures). *Mechanics of Visco-Elastic Media and Bodies*, 1975.
9. Dassault Systèmes. ABAQUS/CAE User's Manual version 6.11, Simulia Corp., Providence, RI, 2011.
10. Kawashima Y, Nishimura M. Study on buckling strength of steel hollow square sections (Effect of welding and cold forming). *Proceedings of the Annual meeting of the Architectural Institute of Japan*, AIJ, Japan, 1973. (In Japanese)
11. Krawinkler H, Zohrei M. Cumulative damage in steel structures subjected to earthquake ground motions. *Computers & Structures*, 1983; 16(1–4): 531–541.
12. Ramberg W and Osgood WR, Description of stress-strain curves by three parameters. Technical Note No. 902, National Advisory Committee For Aeronautics, Washington DC, 1943.
13. Spacone E, Ciampi V, Filippou FC. Mixed formulation of nonlinear beam finite element. *Computers & Structures*, 1996; 58(1): 71–83.
14. Neuenhofer A, Filippou FC. Evaluation of Nonlinear Frame Finite-Element Models. *Journal of Structural Engineering*, 1997; 123(7): 958–966.
15. Scott M, Fenves G. Plastic Hinge Integration Methods for Force-Based Beam–Column Elements. *Journal of Structural Engineering*, 2006; 132(2): 244–252.
16. Suzuki Y, Lignos DG. Development of loading protocols for experimental testing of steel columns subjected to combined high axial load and lateral drift demands near collapse. *10th National Conference on Earthquake Engineering (NCEE)*, EERI, Anchorage, Alaska, 2014.
17. Suita K, Yamada S, Tada M, Kasai K, Matsuoka Y, and Shimada Y. Collapse experiment on 4-story steel moment frame: Part 2 detail of collapse behavior. *14th World Conference on Earthquake Engineering (WCEE)*, Beijing, China. 2008.
18. McKenna F. Object-oriented finite element analysis: Frameworks for analysis, algorithms and parallel computing. *PhD dissertation*, University of California, Berkeley, CA, 1997.
19. Gupta A, Krawinkler H. Prediction of seismic demands for SMRFs with ductile connections and elements. *SAC Background Report*, SAC/BD-99/06, 1999.
20. Elkady A, Lignos DG. Modeling of the composite action in fully restrained beam-to-column connections: implications in the seismic design and collapse capacity of steel special moment frames. *Earthquake Engineering & Structural Dynamics*, 2014; 43: 1935–1954.